# IN-LINE AND OFF-LINE MONITORING OF MULLING PROCESSES

By

SUYANG WU

A thesis submitted to the

Graduate School – New Brunswick

Rutgers, The State University of New Jersey

In partial fulfillment of the requirement

For the degree of

Master of Science

Graduate Program in Chemical and Biochemical Engineering

Written under the direction of

Dr. Rohit Ramachandran

And approved by

_____

_____

_____

_____

New Brunswick, New Jersey

May, 2014

# ABSTRACT OF THE THESIS

In-line and Off-line Monitoring of Mulling Processes

By SUYANG WU

Thesis Director:

Dr. Rohit Ramachandran

The objectives of this study consisted of: (1) determining the optimal instrument set-up of a Near Infrared (NIR) spectrometer and, (2) monitoring and quantifying critical quality attributes (CQAs) of a continuous mulling process. For this, off-line and in-line calibration standards of alumina/nitric acid granules with known water concentrations were prepared. Subsequently, the relationship between sample-detector distance and prediction accuracy was investigated for a JDSU microNIR spectrometer. It was found that the optimal distance was around 15 mm, 15mm of sample thickness and 25 of scan number. Additionally, other set-ups which could be used for in-line monitoring have been investigated including monitoring from the side and/or bottom surface through glass or plastic. Next, after ensuring adequate method accuracy, NIR prediction models were built for the in-line measurement of CQAs: granule water content and agglomerate size.

# Acknowledgement

To try and thank everyone who made my life and work at Rutgers colorful and meaningful is clearly daunting; nevertheless, I will try my best. Foremost, my advisor, Dr. Rohit Ramachandran, for his creative suggestions and patient instructions which have guided me all the way through, and also other members of my thesis committee: Prof. Benjamin Glasser, Dr. Xue Liu and Dr.Aditya Vanarase. Also, I need to express my sincere gratitude to Ph.D. students Krizia Karry and Sarang Oka, postdoctoral associates Dr. Ravendra Singh and Dr. Savitha Panikar for their insightful discussions which gave shape to my thoughts and ideas and their help with various resources. Special thanks to all members of the Catalyst Manufacturing Science and Engineering Consortium for their generous support and thought out advice, especially Dr. Niels Dalskov and Dr. Ninna Halberg Jokil from Haldor Topsoe, Dr. Mingjiang Zhan from W. R. Grace & Co. and Dr. Shizhong Zhao from Clariant. And lastly, the people who made my stay at Rutgers a wonderful one - my fellow group members, roommates and dear friends of the Chemical and Biochemical Engineering (CBE) department – thank you all for the valuable memories; I am truly indebted.

# *Index*

# Chapter 1 Introduction

Inorganic metal-oxide supports offer interesting properties for immobilization of metal complexes, such as mechanical strength, surface area and porosity[1]. Alumina is one of the inorganic supports which are being widely used since a long time in the catalyst industry for various applications including in the petroleum industry[2], petrochemical industry[3], pharmaceutical industry[4], for biofuel[5], and so on. The presence of alumina support[5] and even the structure of alumina[3] could significantly affect the performance of catalysts, for example, as indicated by Luo Sha et al[3]. Catalysts supported on alumina, which are synthesized by ammonia precipitation, exhibit higher activity and selectivity to isobutene than the corresponding catalyst synthesized from hydrochloric acid reflux. Due to its importance and large demand in the catalyst industry, the large-scale manufacturing of extrudable alumina to achieve desired porosity and surface area is a challenging problem in the scientific and industrial community.

Usually, the production of alumina is processed in three steps: mulling, extrusion and calcination. Mulling can be used to improve the flowability and with the help of a peptizing agent and at high temperature, the primary particle size would decrease, thus, increasing the porosity and shaping the pore size distribution. Extrusion is a commonly used shaping process in many industries, and it is also used in catalyst industry since extrudate catalyst support is much easier to handle and recycle. The main condition that the extrusion compounds have to fulfill is that they had to have

sufficient plasticity[8]. Alumina is a known non-plastic material and, therefore, extrusion of alumina pastes require processing additives such as binder and lubricant agents to impart plasticity and flow characteristics, which is another reason for mulling application in catalyst support production. In the mulling process, water or nitric acid solution could be used as the binder, whose amounts have significantly effect on the plasticity, which makes the monitoring of water content extremely meaningful.

In plant scale manufacturing, companies mainly perform batch processing since the batchwise machinery is already installed and is more flexible, in terms of both machine application and productivity adjustment. However, continuous processing is more suitable for manufacturing based on Quality-by-Design (QbD). It is well-established in the chemical, cosmetics and food industry, and has many advantages [6-7]: Firstly, it is much easier to scale up, which could be achieved by simply running the process longer, thus potentially leading to labor and cost savings. . Secondly, it could prevent segregation problems that can be caused by the handling and storing between different processes. Thirdly, this would save space and reduce the need for manual operators.

During recent years, vibrational spectroscopic techniques like Near Infrared (NIR) combined with multivariate calibration routines have become increasingly important process analyzers in the pharmaceutical industry [1-24]. These analyzers offer several advantages over conventional wet chemistry techniques, which include

non-invasiveness, little or no sample preparation and rapid measurements. Raman and NIR sensors can provide critical quality information during different stages of the active pharmaceutical ingredient (API) and drug product manufacturing, and are commonly employed during raw material dispensing, chemical reactions (mostly Raman), granulations, drying (mostly NIR) and powder blending.[10]

Water shows a very strong absorption in the NIR and is thereby the ideal analyte for this technology. NIR is very successfully used for determination of water content in the food, chemical and pharmaceutical industries.[11] Measurements in solids, liquids and pastes are possible without sample preparation; if required, this is possible online. A wide range of probes for both diffuse reflection and transmission measurements are available.[12] Therefore, Near Infrared Spectroscopy has been selected as a technique to develop in this thesis.

# Chapter 2 Near Infrared Based Sensing

## 2.1 Near Infrared Introduction

Near Infrared Spectroscopy (NIRS) is a spectroscopic method in which near infrared region of radiation (800 – 2500 nm) is utilized. The frequency range covers mainly overtones and combinations of the lower-energy fundamental molecular vibrations that include at least one X-H bond vibration. However, they are significantly weaker in absorption cross-section, compared with the fundamental vibrational bands from which they originate. Fortunately, an advantage, in terms of analytical specificity of NIR, is the sensitivity of the frequency and intensity of these X-H NIR absorption bands to near neighbors in the molecular structure. The local electronic environment has particularly strong influence on the X-H bond force constants and from this derives remarkably high information content in spectra. The functional groups almost exclusively involved in NIR are those involving the hydrogen atom: C-H, N-H, O-H, which are the overtones and combinations of their fundamental frequencies in the mid-IR and produce absorption bands of useful intensity in the NIR. And this is why Near Infrared is quite useful in quality control, and it is widely used in agricultural food, pharmaceutical, cosmetic and many other industries.

One of the analyzer formats used to achieve full-spectrum information is the scanning grating monochromator. This is a robust piece of equipment, normally based on a concave holographic grating, controlled via industrial motor drive and optical tungsten-halogen source at 2800 K and suitable detector can achieve a near-perfect

match of the monochromator throughput with detector sensitivity and hence very high signal-to-noise ratio (SNR).

An obvious extension of the scanning monochromator is the grating polychromator, fitted with a photodiode array (PDA). Whilst this system still requires an entrance slit to the concave grating, the exit slit is replaced with a PDA, which allows for a multiplex measuring advantages including shorter response time and high SNR.

A further example of high-throughput full-spectrum device is the tunable filter instrument, normally based on an acousto-optical tunable filter (AOTF). In this case, no entrance slit is required. The AOTF filter is based on the use of a carefully oriented briefringent crystal, optically transparent across NIR. The crystal is driven by an RF-powered piezoelectric transducer, which sets up an acoustic wave that propagates through the crystal and interacts with the incident broadband NIR radiation.

Finally, in the field of full-spectrum NIR methods, Fourier transform near-infrared (FTNIR) analyzers are included. An FTIR device is, in effect, an optical modulator which allows wavelength encoding. The input beam is unmodulated broadband NIR, and the exit beam from the interferometer is still broadband NIR, but with each optical frequency uniquely amplitude-modulated in the acoustic frequency range. This allows the detector signal (which is a combination of signals from all the incident broadband NIR frequencies) to be decomposed using Fourier transform, and the individual amplitudes of each optical frequency in the broadband input signal to be obtained. The system thus has no input or output restriction other than a resolution

defining Jacquinot stop. The uniquely defining feature of FTIR methods in NIR is that they all contain some inherent form of direct wavelength registration. Most practical devices employ a visible frequency laser to define the optical retardation sampling interval. This translates directly into the frequency axis of the recorded spectrum, linked intimately with the known HeNe laser frequency.

These four very different NIR technologies represent the mainstream analyzer types and they also cover the main types of established commercially available analyzers. In the offline monitoring part of this thesis, we used Antaris FTNIR distributed by Thermo, and JDSU MicroNIR 2200 spectrometer, which is a polychromator used in inline monitoring.

## 2.2 Multivariate Analysis

Multivariate analysis is based on the statistical principle of multivariate statistics, which involves observation and analysis of more than one statistical outcome variable at a time. Since the spectrum generated by Near Infrared is actually a matrix with one row and hundreds of columns (depends on resolution wavelength range) and the information which could be used for either substance discrimination or quantification is a range including more than one wavelength, therefore multivariate analysis is required to extract the information from Near Infrared spectra. In this thesis, Unscrambler and TQanalys are the software used for spectra interpretation. And PCA (principal component analysis) and PLS (partial least square) are the methodology mainly used in this thesis.

### 2.2.1 Principal Component Analysis

PCA is a bilinear modeling method that provides an interpretable overview of the main information contained in a multidimensional table. It is also known as a projection method, because it takes information carried by the original variables and projects them onto a smaller number of latent variables called Principal Components (PC). Each PC explains a certain amount of the total information contained in the original data and the first PC contains the greatest source of information in the data set. Each subsequent PC contains, in order, less information than the previous one.

By plotting PCs, important sample and variable interrelationships can be revealed, leading to the interpretation of certain sample groupings, similarities or differences.

When a measured variable exhibits large systematic variation, this is attributed to information. If a variable exhibits very little variation, it can be concluded there is no information associated with it and it may be contributing to "noise". PCA aims to extract the information from a data table and disregard the noise.

In matrix representation, the model with a given number of components has the following equation:

$$X = TP^T + E$$

where $T$ is the scores matrix, $P$ the loadings matrix and $E$ the error matrix. These terms will be explained in more detail in this document.

The combination of scores and loadings is the structured part of the data: the part that

is most informative. What remains is called error or residual, and represents the fraction of variation that cannot be modeled well. By multiplying the scores and the loadings together, the entire structure of the original data set can be reconstructed and hopefully, only a small residual is left, consisting of random fluctuations which cannot be meaningfully modeled.

Each component of a PCA model is characterized by three complementary sets of attributes: scores, loadings and explained variance.

Scores describe the properties of the samples and are usually shown as a map of one PC plotted against another. However, PCs can be plotted as line plots for describing time evolving processes.

Loadings describe the relationships between variables and may be plotted as a line (commonly used in spectral data interpretation) or a map (commonly used in process or sensory data analysis).

Explained variances are error measures that tell how much information is taken into account by each PC.

Usually, scores plots coupling with Hotelling Circle could be used for the classification of samples, outlier detection and process control. Loading plot which tells the effect of variables could be used for design of experiment, although no significance could be determined by this method, the bright side is each run of experiments doesn’t have to be fixed. Explained variance could tell the adequacy of

one model, and if it's not high, it remind you to find the variable which could have significant effect on the response.

### 2.2.2 Partial Least Square Regression

Partial Least Squares Regression (PLSR), also sometimes referred to as Projection to Latent Structures or just PLS, models both the X- and Y-matrices simultaneously to find the latent (or hidden) variables in X that will best predict the latent variables in Y. These PLS components are similar to principal components, but will be referred to as factors.

The model generated by PLS could be used for future quantification of certain substance, but one thing is very important: Good models are generated from good data! If either the X or Y data are non-representative of future conditions, or if they were collected under poor conditions, then the results of the PLSR model may be useless.

## 2.3 Near Infrared Liquid Content Standards

As stated in 2.2, to predict the amount of certain chemical substance, one standard (or model) with different known amount has to be made. Thus, many standards of water had been made and they were validated by the prediction of samples with unknown water content.

### 2.3.1 Materials, Equipment and Methods

Materials: Purified water, nitric acid and DISPERAL boehmite alumina manufactured by Sasol were used in all experiments.

Equipment: Thermo Antaris Near Infrared spectrometer, VWR vortex, JDSU Miniature spectrometer, Labram Acoustic Mixer

Methods: The standard curve was built by measuring NIR absorbance curve from samples with known water content achieved by adding different amounts of water into fixed amount of alumina. The water percentage varied from 45% to 65% with an interval of 2%. Due to sample loss from scratching, a correction factor was applied. A calibration model was built using multivariate analysis that was then validated using a test set, which consisted of several samples with random amounts of water within the calibration range.

Many standards including 0.5% nitric acid standard, 1% nitric acid standard for Antaris NIR, and water standard for JDSU Miniature NIR have been created. Calibration ranges for some of them have been expanded from 0% to 75% (initially 45% to 65%).

### 2.3.2 Antaris Water Standard

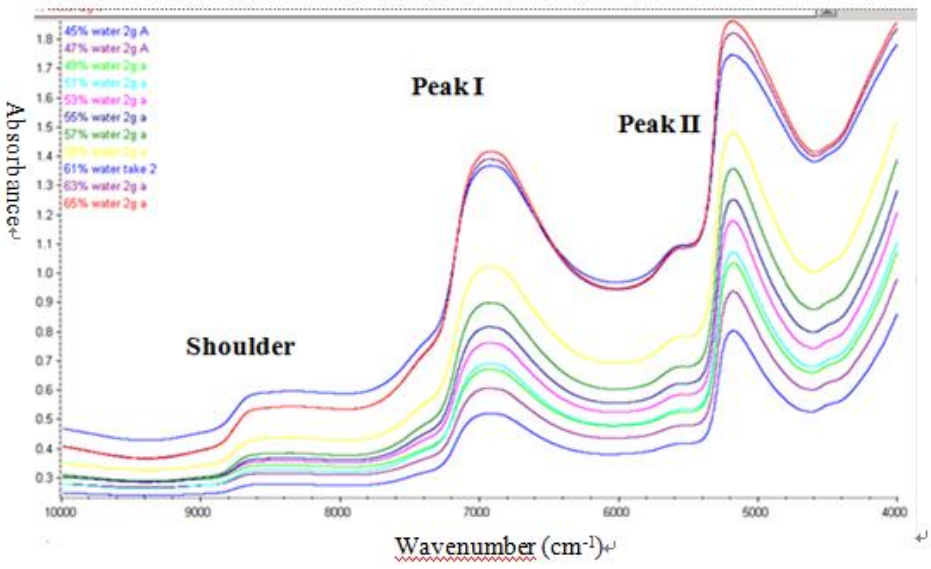


Figure 2.1. Spectra for Antaris water standard

Figure 2.1 shows the curves detected by NIR. Two significant peaks could be found around 7000 $cm^{-1}$ and 5000 $cm^{-1}$, and a shoulder is also spotted around 8600 $cm^{-1}$. Initially, peaks I and II were assumed to represent water and alumina, respectively, whereas the shoulder assumed to have no significance. Later, upon detailed analysis of the data using the TQ Analyst software, an interesting fact was observed: Both the peaks and the shoulder correlated to water content very well. Their correlation coefficients are all above 0.996. Keeping in mind the limited wavelength range for the JDSU (5800-11,000 $cm^{-1}$), 6700-7150 $cm^{-1}$ was selected to be suitable for water content prediction models.

Figure 2.2 is generated by TQanalyst to show the difference between the actual water content measured from the sample and the water content calibrated by TQanalyst. Points at 0.63 and 0.65 are clearly deviated from the curve, since alumina at that water

content is very sticky and minor operation mistakes could lead to such deviations.

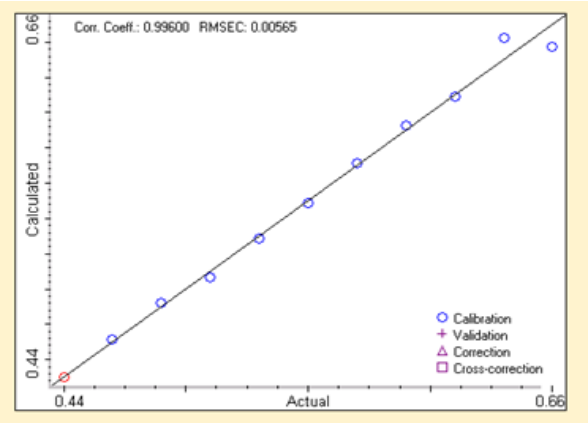


Figure 2.2. Plot of Actual Water Content vs Calculated Water Content

Table 2.1 shows the result of actual water content and calculated water content. It can be seen that every point except the last two agree perfectly well.

Table 2.1. Results of Calculated and Actual Water Content

Calibration Results Table

| Index | Spectrum Title | Actual | Calculated | Diff. x Path |
|---|---|---|---|---|
| 3 | 45% water 2g A | 0.45 | 0.45 | 0.00 |
| 4 | 47% water 2g A | 0.47 | 0.47 | 0.00 |
| 5 | 49% water 2g a | 0.49 | 0.49 | 0.00 |
| 6 | 51% water 2g a | 0.51 | 0.51 | 0.00 |
| 7 | 53% water 2g a | 0.53 | 0.53 | 0.00 |
| 8 | 55% water 2g a | 0.55 | 0.55 | 0.00 |
| 9 | 57% water 2g a | 0.57 | 0.57 | 0.00 |
| 10 | 59% water 2g a | 0.59 | 0.59 | 0.00 |
| 12 | 61% water take 2 | 0.61 | 0.61 | 0.00 |
| 13 | 63% water 2g a | 0.63 | 0.64 | 0.01 |
| 14 | 65% water 2g a | 0.65 | 0.64 | -0.01 |

Validation was achieved by detecting the water content of samples which constituted a known amount of water. The sample was newly prepared for the purpose of validation.

Table 2.2. Validation result of 20130226-water standard

| Water Content | 52% | 55% | 58% |
|---|---|---|---|
| 1 | 0.52 | 0.55 | 0.56 |

| | | | |
|---|---|---|---|
| 2 | 0.52 | 0.54 | 0.57 |
| 3 | 0.51 | 0.55 | 0.58 |

This standard is expanded to 0% to 75% later and its corresponding coefficient is 0.99963, and its validation result is given in Table 2.3:

Table 2.3. Validation result of 20130226-water standard expanded

| Water Content | 52% | 55% | 58% |
|---|---|---|---|
| 1 | 0.52 | 0.55 | 0.51 |
| 2 | 0.52 | 0.54 | 0.51 |
| 3 | 0.52 | 0.55 | 0.52 |

Comparing table 2.2 and table 2.3, two conclusions can be made as follows:

- For a known range, the unexpanded (narrow) range of moisture content distribution worked well.
- For a range lower than the known range, the expanded model was used and there were deviations observed from the actual moisture content.

### 2.3.3 Antaris 0.5% Nitric Acid Standard

The corresponding coefficient was 0.99825, and its validation result is given in Table 2.4.

Table 2.4. Validation result of Antaris 0.5% nitric acid standard

| Water Content | 52% | 55% | 58% |
|---|---|---|---|
| 1 | 0.52 | 0.55 | 0.56 |
| 2 | 0.52 | 0.55 | 0.55 |
| 3 | 0.52 | 0.55 | 0.58 |

Table 2.5. Validation result of 0.5% nitric acid sample using Antaris water standard

| Water Content | 52% | 55% | 58% |
|---|---|---|---|
| 1 | 0.53 | 0.52 | 0.57 |
| 2 | 0.53 | 0.54 | 0.58 |
| 3 | 0.53 | 0.54 | 0.58 |

Comparing table 2.4 and table 2.5, it can be concluded that Nitric acid standard is necessary, since the 0.5% nitric acid liquid content prediction given by water standard deviated from the actual liquid content.

### 2.3.4 Antaris 1% Nitric Acid Standard

The corresponding coefficient is 0.99777, and its validation result is:

Table 2.6. Validation result of 1% nitric acid standard expanded

| | 10% | 20% | 52% | 55% | 58% |
|---|---|---|---|---|---|
| 1 | 0.06 | 0.22 | 0.55 | 0.55 | 0.6 |
| 2 | 0.11 | 0.22 | 0.52 | 0.54 | 0.61 |
| 3 | 0.08 | 0.22 | 0.52 | 0.53 | 0.6 |

### 2.3.5 Micro NIR (JDSU) Water Standard

This standard could be used during continuous mulling due to the excellent R-square value and low RMSECV.

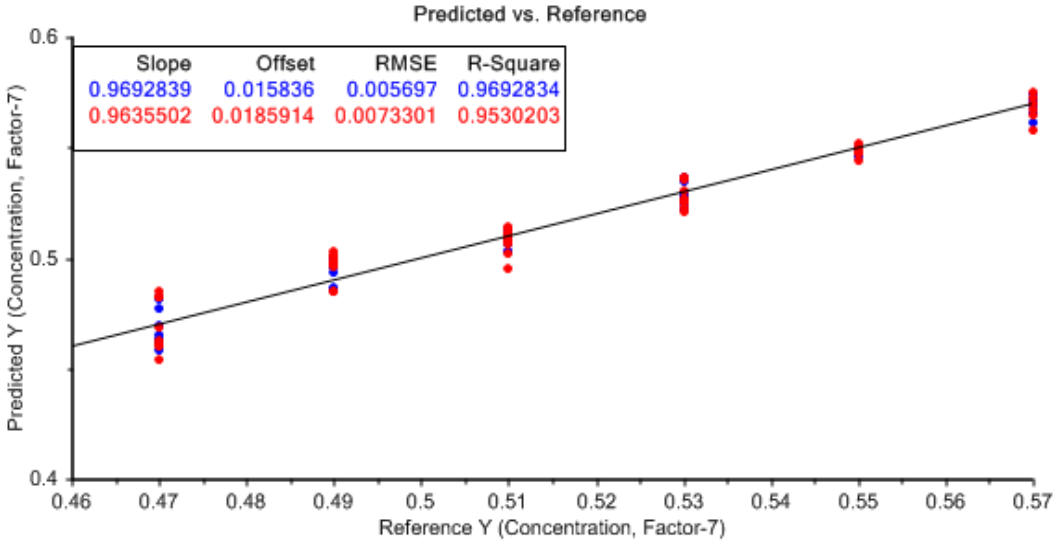


Figure 2.3. Predicted vs reference plot of JDSU NIR standard

## 2.4 Near Infrared Particle Size Standard

One articles[10] points out that NIR can be used to measure particle size. This is achieved by baseline-corrected absorbance (ΔA), which is given in the form of the following equation:

$$\Delta A = A_x - A_y$$

The 1740 nm signal was used for correction of the background level and 2145 nm was

applied as a particle size measurement wavelength

### 2.4.1 Materials, Equipments and Methods

Materials: Purified water and DISPERAL boehmite alumina manufactured by Sasol were used in this experiment.

Equipments: Thermo Antaris Near Infrared spectrometer, KG-5 batch granulator, Malvern Laser diffraction, sieving device and oven.

Methods:

1. Mulling: To produce granules of different particle size, a batch granulator had

   been used.

2. Drying: For better sieving, the material was dried at 90 ℃ until only bound water remained.

3. Sieving: This separated all granules based on size differences.

4. NIR Measurement: This created a dry, particle size single-variable standard.

5. The particle size was measured by Malvern Laser Diffraction to give the true value of particle size (d50 used).

### 2.4.2 Results

Laser Diffraction: After sieving and NIR Measurement, laser diffraction was used to verify the exact particle size. Both methods were in general agreement.

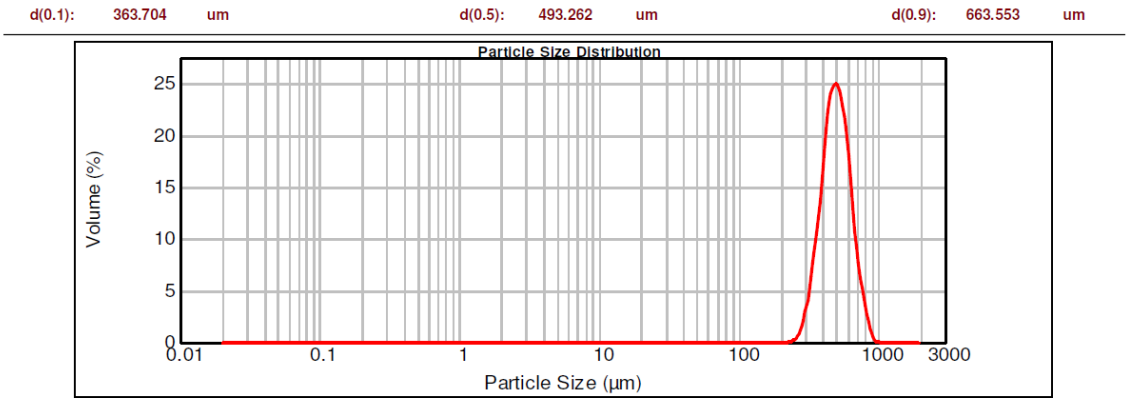


Figure 2.4. Particle size profile of particles which were retained on No. 40 pan and passed through No. 35 pan (from 420 to 500 microns)

Neither R-square nor RMSECV of the method suggested in literature was optimal, so different ranges (wavelength) had been attempted. The difference between the original spectra plot and first derivative plots had been compared to determine the range. The first derivative method, supposedly, eliminates physical properties of samples, like particle size. Several ranges observed with a large difference between these two plots had been analyzed by PCA. The 4200-4600 $cm^{-1}$ range was decided to be used.

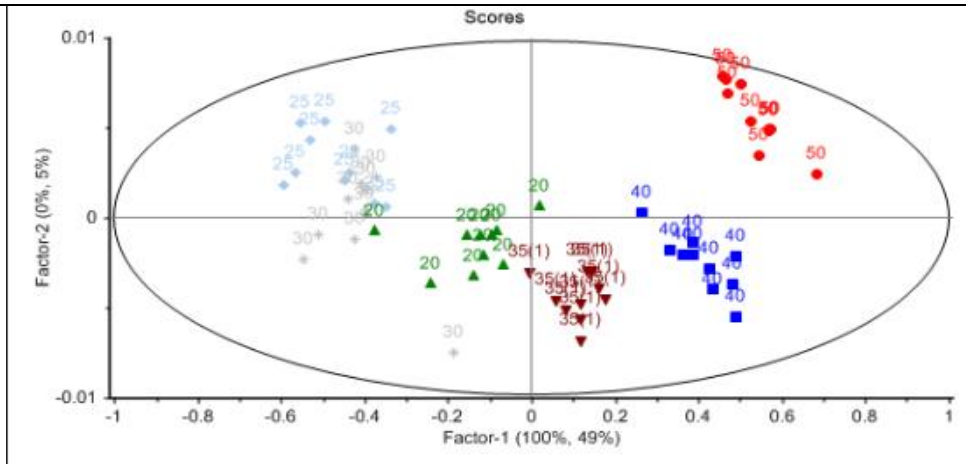


Figure 2.5. PCA result of samples with different particle size in the 4200-4600 $cm^{-1}$ range

In Figure 2.5, the pattern indicates that particles retained on the same sieving pan were grouped together and were distinguishable from other groups indicating that this range managed to classify the particle size effects.

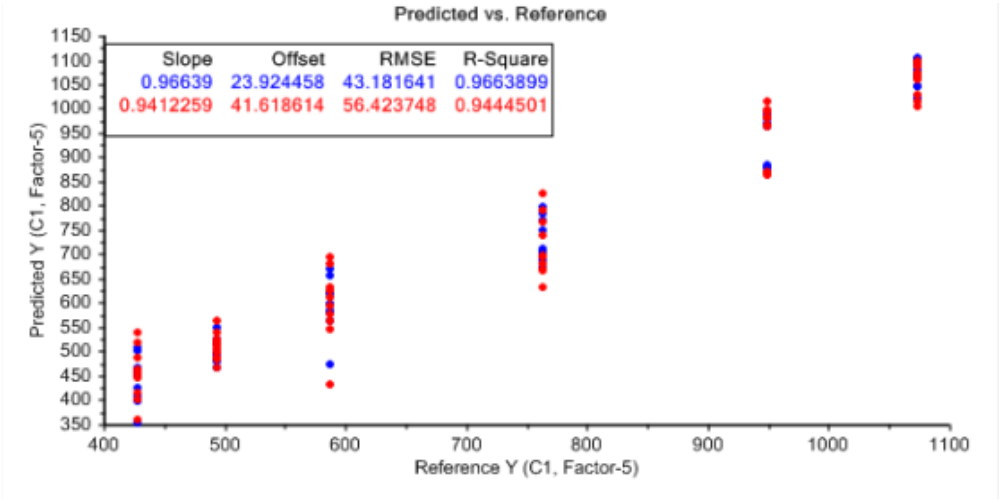


Figure 2.6. Predicted vs reference plot of particle size standard

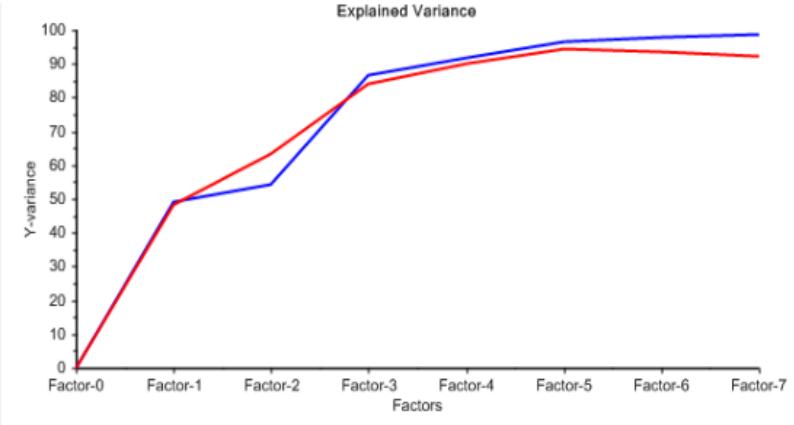


Figure 2.7. Explained variance plot of particle size standard

This plot indicates that more than 90% percent of variance could be explained by five factors, with room for improvement.

Based on these results, it could be concluded that:

1. The standard has been successfully created.
2. To improve the model, a narrower range (wavelength and sieve range) would be needed.
3. The cross validation results were not ideal (high RMSECV), prediction mode validation could be attempted instead.

# Chapter 3 Design of Optimal Operational Condition of Near Infrared

To determine the optimal operational conditions for MicroNIR 2200 spectrometer (JDSU), several experiments have been performed to investigate the effect of sample detector distance, sample thickness, scan number, sample agglomerate size, sample surface roughness, place orientation and type of transparent material the light beam could go through.

## 3.1 Design of Experiment to identify optimal Distance, Sample Thickness and Scan Number

During operation, the granulation process may cause dusting, which could lead to containment and clogging of NIR sensor and inaccurate prediction. Therefore, it would be better if the Near Infrared detector could be away from dusting sample for a reasonable distance. Also, the thickness of sample and scan number (the times of scanning made by detector to give the final spectrum) could also jeopardize results. Therefore, all these three parameters need to be investigated to identify the optimum values.

In this study, two experiments have been designed to determine the effect of four variables: integration time, distance between sample and detector, sample thickness and number of sample. Integration time is the length of time that detector can capture light, and number of sample represents how many spectra the detector will take to

give an average final spectrum. As suggested by NIR sensor manufacturer (JDSU), highest signal noise ratio can only be achieved by setting at the right integration time for certain sample detector distance. In the first experiment, the effect of varying distance to a model at fixed integration time has been investigated. The objective of that experiment is to determine at what degree of variation of distance will jeopardize the prediction. And the second experiment is a DOE finished with all four variables mentioned above, and to give fair comparison of each distance. Only the optimal combination of integration time and distance giving highest signal noise ratio has been considered for second experiment.

### 3.1.1 Experimental Set-up

Equipment: Height-adjustable support, petri-dishes of different thickness (5, 10 and 15mm), vernier caliper, JDSU Miniature NIR spectrometer.

Software: Minitab (DOE analysis), IRSE (Spectra recording), Unscrambler (Data processing)

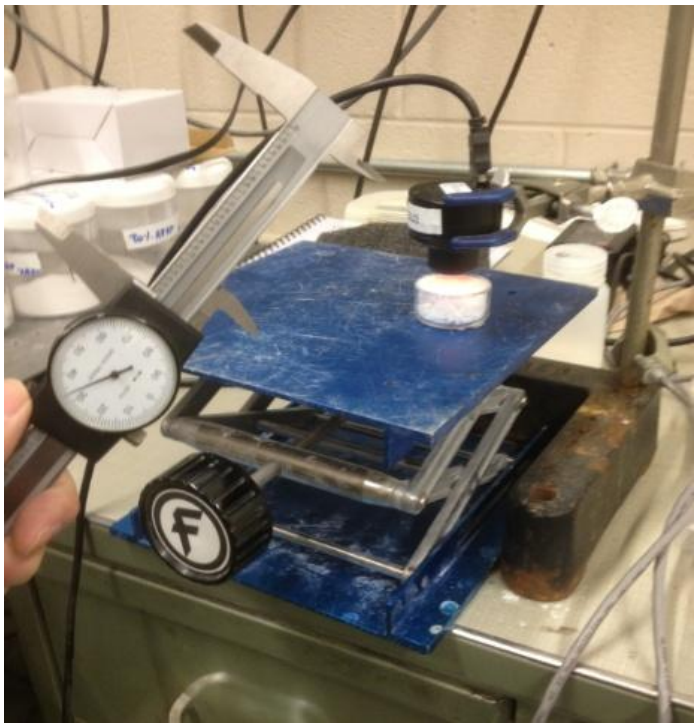

Figure 3.1. Experimental Setup

The distance between JDSU and sample = Height of JDSU – Height of petri-dish – Height of support (heights were measured by a Vernier caliper)

Eight prediction models at different distances had been prepared to determine their accuracy toward the same sample. The models were built at 3, 6, 9, 12, 15, 18, 21 and 24 mm distances. For each of these models, nine different distances had been tested. The distance ranged from 6mm below the distance of the model being built to 6mm above that model with an interval of 1.5 mm between the distances. As an example, for the 15mm model, the prediction sample distances were at 9, 10.5, 12, 13.5, 15, 16.5, 18, 19.5 and 21mm from the JDSU.

### 3.1.2 Distance effect experiment

In this experiment, only one prediction model was used, and this model was created

with an integration time of 9000 μs and an initial sample detector distance of 3mm. This distance was varied to determine what gave an optimum prediction. The difference between true value (determined by LOD at 130 ℃) and the prediction was set as the response in the multivariate analysis.

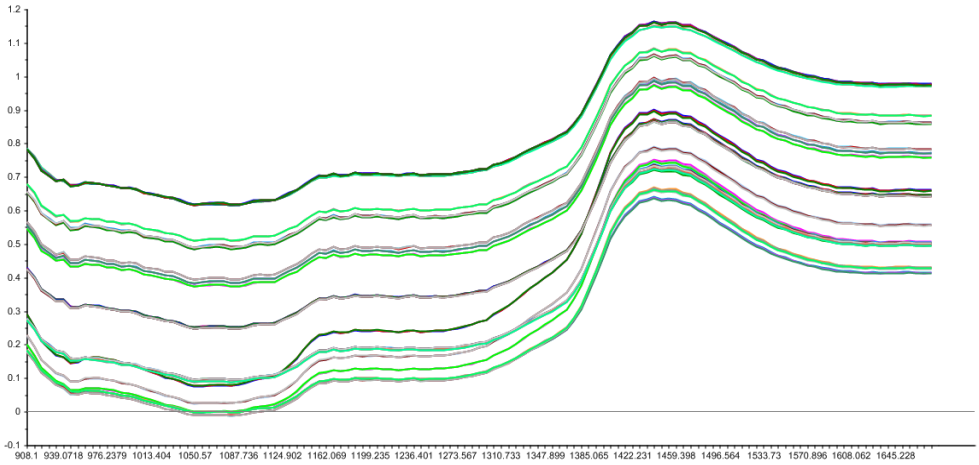


Figure 3.2. 3mm Different Distance Spectra

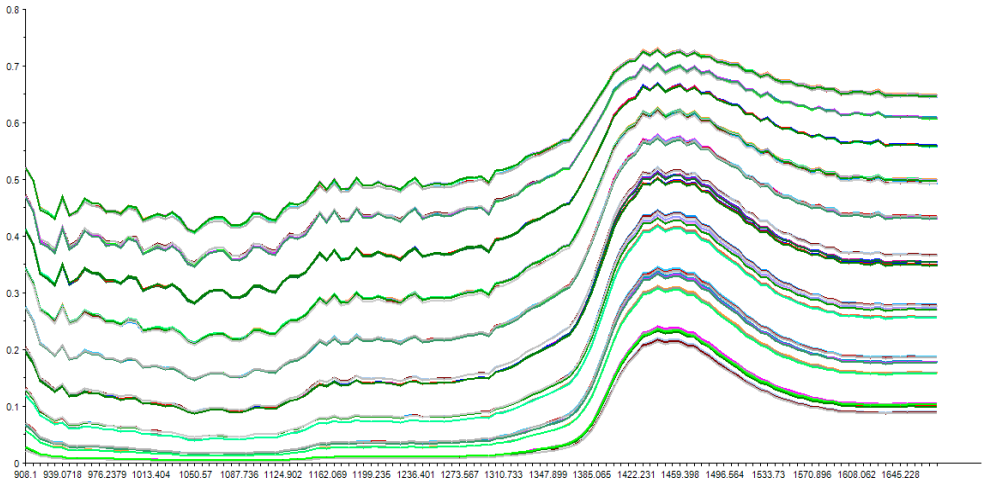


Figure 3.3. 9mm Different Distance Spectra

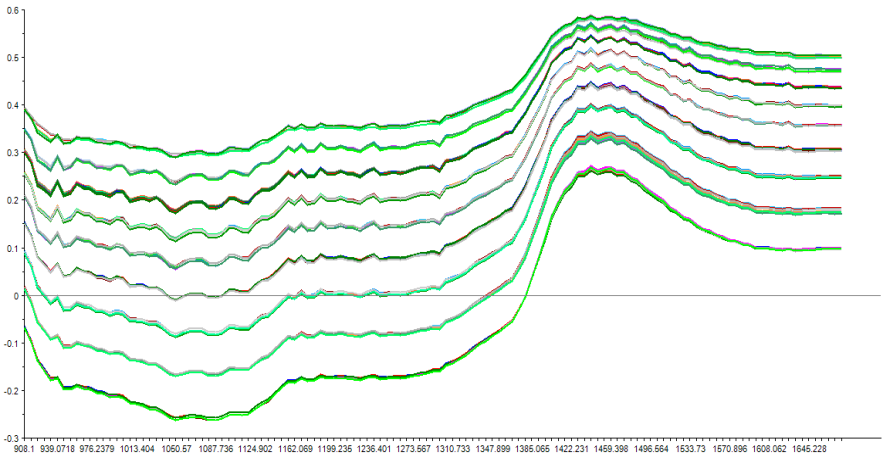


Figure 3.4. 15mm Different Distance Spectra

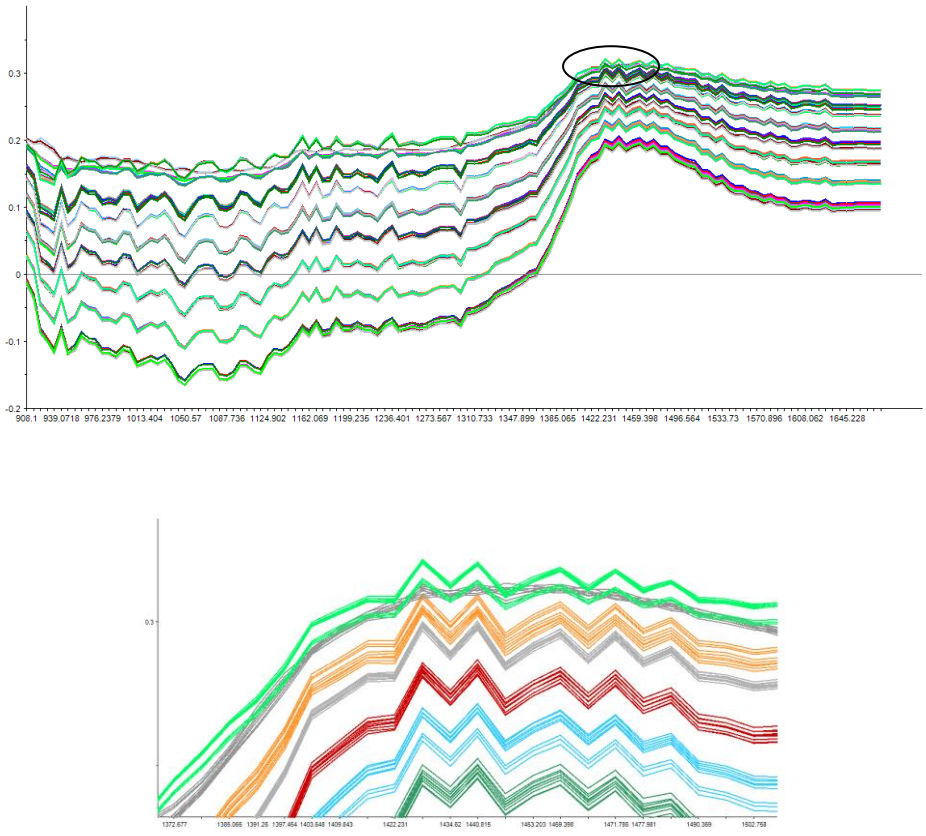


Figure 3.5. 24mm Different Distance Spectra (upper) Magnified section of circled area.(lower)

Several conclusions can be made by comparing the spectra:

- The absorbance value decreases as the distance between sample and JDSU increases.
- The spectra were not smooth at higher distance.
- In figure 3.5(b), the spectra at different distances were supposed to be clustered into different groups, but instead there was some overlap, which might represent the “breakdown point”
- Integration time increases as the distance increases.
- The comparison of spectra from same and different distances indicated that distance could significantly change the absorbance value of the baseline.

**Models:**

The resulting models were reliable since they had R-square values close to 1 and RMSE lower than 0.003.

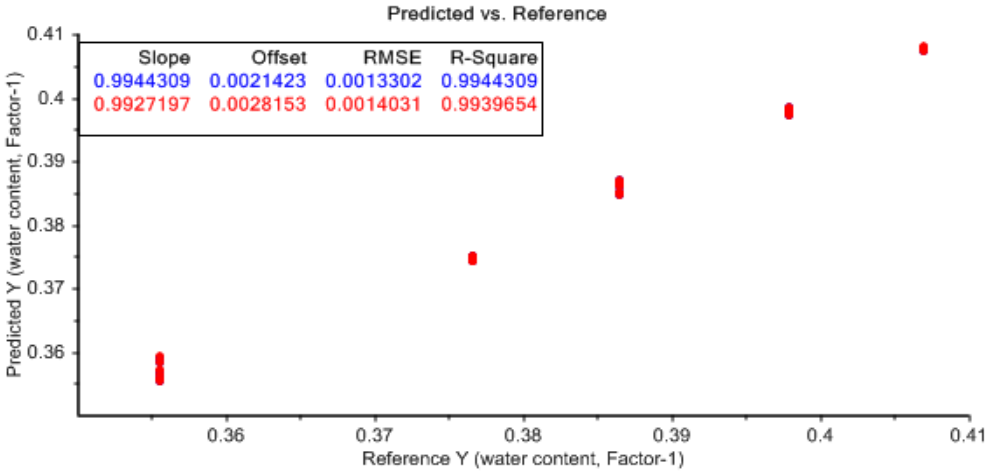


Figure 3.6. Reference vs Predicted for 15mm water model

**Pretreatments:**

To determine whether pretreatment (Savitzky Golay first derivative, 1st order polynomial and with 15 points window) had any improvement on the prediction accuracy, comparisons to the 15mm model were made.

(a)

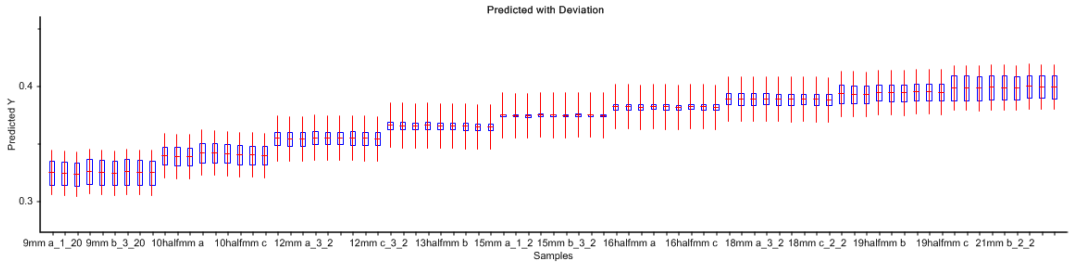


(b)

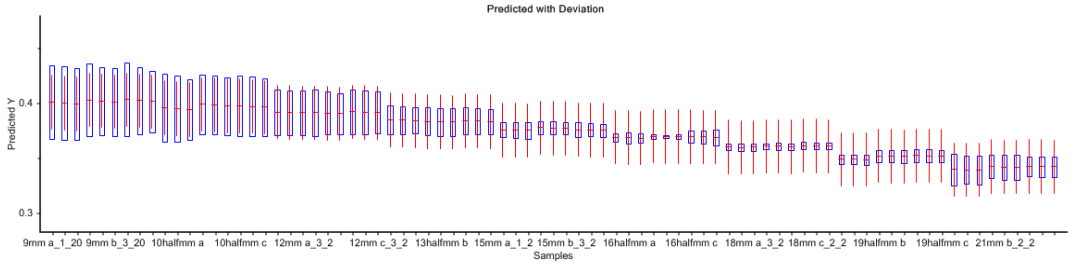


Figure 3.7. Prediction with deviation plot for 15mm model (a) Prediction with deviation plot for 15mm model (b)

Table 3.1. Prediction result of sample at different distance given by 15mm model of different pretreatment

| | | Treated (SGolay) | | Untreated | |
|---|---|---|---|---|---|
| Distance(mm) | reference | Y predicted | Deviation | Y predicted | Deviation |
| 9.0 | 0.363682 | 0.400717 | 0.031822 | 0.324083 | 0.010466 |
| 10.5 | 0.36601 | 0.395892 | 0.027601 | 0.339701 | 0.008093 |
| 12.0 | 0.368224 | 0.390574 | 0.019994 | 0.353962 | 0.005725 |
| 13.5 | 0.371437 | 0.382929 | 0.01244 | 0.3647 | 0.003057 |

| | | | | | |
|---|---|---|---|---|---|
| 15.0 | 0.371471 | 0.375382 | 0.006265 | 0.374044 | 0.000994 |
| 16.5 | 0.373814 | 0.368399 | 0.004204 | 0.381368 | 0.002228 |
| 18.0 | 0.375419 | 0.359825 | 0.002997 | 0.387993 | 0.004765 |
| 19.5 | 0.376306 | 0.350201 | 0.005271 | 0.393493 | 0.007355 |
| 21.0 | 0.378703 | 0.340586 | 0.011272 | 0.398291 | 0.010338 |

In Table 3.1, reference values are the water contents obtained from Loss on Drying (LOD) method, regarded as true values. Y predicted water content values are predicted by the model while the deviation values simply represent the standard deviations.

Conclusions that can be drawn from this comparison:

- Both methods gives accurate prediction at 15 mm
- The pre-treated data did not give as good results in comparison to data that was untreated. Due to this, untreated data was used for building further models.

**Varying Distance:**

Table 3.2. Prediction result of sample at different distance given by 3mm model

| Distance(mm) | Reference | Y predicted | Deviation | Difference |
|---|---|---|---|---|
| 0 | 0.393059 | 0.403781 | 0.02524 | 0.010722 |
| 1.5 | 0.324244 | 0.389906 | 0.01379 | 0.065661 |
| 3 | 0.365066 | 0.393463 | 0.010729 | 0.028397 |
| 4.5 | 0.367727 | 0.403183 | 0.005251 | 0.035457 |
| 6 | 0.372821 | 0.409694 | 0.005811 | 0.036873 |
| 7.5 | 0.371296 | 0.402569 | 0.007867 | 0.031273 |
| 9 | 0.37341 | 0.373513 | 0.015283 | 0.000103 |

Table 3.3. Prediction result of sample at different distance given by 9mm model

| Distance(mm) | Reference | Y predicted | Deviation | Difference |
|---|---|---|---|---|
| 3 | 0.351856 | 0.318911 | 0.020438 | 0.032946 |
| 4.5 | 0.354222 | 0.346502 | 0.019297 | 0.00772 |
| 6 | 0.358536 | 0.366727 | 0.020904 | 0.008191 |
| 7.5 | 0.362018 | 0.373338 | 0.024233 | 0.01132 |
| 9 | 0.364685 | 0.376272 | 0.02428 | 0.011587 |
| 10.5 | 0.367951 | 0.374805 | 0.026022 | 0.006854 |
| 12 | 0.370215 | 0.37251 | 0.026496 | 0.002296 |
| 13.5 | 0.372794 | 0.368145 | 0.025082 | 0.00465 |
| 15 | 0.376509 | 0.360277 | 0.020526 | 0.016231 |

Table 3.4. Prediction result of sample at different distance given by 15mm model

| Distance(mm) | Reference | Y predicted | Deviation | Difference |
|---|---|---|---|---|
| 9 | 0.363682 | 0.324083 | 0.010466 | 0.037035 |
| 10.5 | 0.36601 | 0.339701 | 0.008093 | 0.029882 |
| 12 | 0.368224 | 0.353962 | 0.005725 | 0.022351 |
| 13.5 | 0.371437 | 0.3647 | 0.003057 | 0.011492 |
| 15 | 0.371471 | 0.374044 | 0.000994 | 0.003911 |
| 16.5 | 0.373814 | 0.381368 | 0.002228 | 0.005415 |
| 18 | 0.375419 | 0.387993 | 0.004765 | 0.015594 |
| 19.5 | 0.376306 | 0.393493 | 0.007355 | 0.026105 |
| 21 | 0.378703 | 0.398291 | 0.010338 | 0.038116 |

Table 3.5. Prediction result of sample at different distance given by 24mm model

| Distance(mm) | Reference | Y predicted | Deviation | Difference |
|---|---|---|---|---|
| 18 | 0.372982 | 0.380253 | 0.032791 | 0.007271 |
| 19.5 | 0.37483 | 0.379672 | 0.025832 | 0.004842 |
| 21 | 0.378021 | 0.376514 | 0.018684 | 0.001506 |
| 22.5 | 0.379649 | 0.373563 | 0.010733 | 0.006085 |
| 24 | 0.381187 | 0.371448 | 0.006799 | 0.009739 |

| | | | | |
|---|---|---|---|---|
| 25.5 | 0.382565 | 0.368063 | 0.008142 | 0.014502 |
| 27 | 0.383655 | 0.363318 | 0.014678 | 0.020336 |
| 28.5 | 0.386425 | 0.351414 | 0.022664 | 0.035011 |
| 30 | 0.385803 | 0.35341 | 0.024041 | 0.032393 |

Following conclusions have been made:

- Predictions at 3mm were not accurate, although, predictions at 9mm or longer were much more accurate.
- 15mm was found to be the optimum distance due to its lowest Y difference
- Deviation was usually small around the model preparation distance.

### 3.1.3 DOE of four variables

**Four variables**

Integration time (int time), distance, scan number and sample thickness has been considered for study. Among these variables, integration time and distance were found to have a strong interaction. As discussed in the previous section, highest signal-to-noise ratio can only be achieved by setting the right integration time for specific sample-detector distance. Therefore, to give fair comparison of each distance, only the optimal combination of integration time and distance giving highest signal noise ratio was used in the second experiment. Thus, a new variable representing the combination of integration time and distance was created, called int-dis. The optimal combination used in this experiment is listed in Table 3.6, which was determined by calibrating a spectrolon (a white disk used as reference) to give 50-60K.

Table 3.6. The optimal combination of integration time and distance used in DOE of four variables

| Int-dis | Int time(μs) | Distance(mm) |
|---|---|---|
| Low level (-1) | 34000 | 9 |
| Medium level (0) | 75000 | 15 |
| High level (1) | 125000 | 21 |

Table 3.7. All variables used in DOE of four varibles

| | Int-dis | Scan number | Sample thickness (mm) |
|---|---|---|---|
| Low level | -1 | 25 | 5 |
| Medium level | 0 | 50 | 10 |
| High level | 1 | 75 | 15 |

**Responses:**

The response used in this study was the difference between true value (determined by LOD at 130℃) and the prediction. The objective of this study was to find the optimized setting of variables to minimize this response.

**DOE:**

Table 3.8. DOE run table

| Standard Order | Run Order | Int-dis | Scan number | Sample thickness (mm) | Prediction – true value difference | Deviation |
|---|---|---|---|---|---|---|
| 4 | 1 | 1 | 75 | 10 | 0.0067700 | 0.0065595 |
| 7 | 2 | -1 | 50 | 15 | 0.0036574 | 0.0064876 |
| 1 | 3 | -1 | 25 | 10 | 0.0039953 | 0.0058358 |
| 8 | 4 | 1 | 50 | 15 | 0.0195654 | 0.0120493 |
| 3 | 5 | -1 | 75 | 10 | 0.0067050 | 0.0083772 |

| | | | | | | |
|---|---|---|---|---|---|---|
| 6 | 6 | 1 | 50 | 5 | 0.0071823 | 0.0120963 |
| 15 | 7 | 0 | 50 | 10 | 0.0076744 | 0.0045620 |
| 14 | 8 | 0 | 50 | 10 | 0.0063972 | 0.0042981 |
| 2 | 9 | 1 | 25 | 10 | 0.0144328 | 0.0104166 |
| 11 | 10 | 0 | 25 | 15 | 0.0002820 | 0.0038985 |
| 12 | 11 | 0 | 75 | 15 | 0.0020793 | 0.0040238 |
| 13 | 12 | 0 | 50 | 10 | 0.0015597 | 0.0038432 |
| 9 | 13 | 0 | 25 | 5 | 0.0006170 | 0.0038824 |
| 10 | 14 | 0 | 75 | 5 | 0.0004370 | 0.0037262 |
| 5 | 15 | -1 | 50 | 5 | 0.0058594 | 0.0145700 |

Standard order is the ID of each run

Run order: the experiment is implemented at a randomized order to avoid bias.

**Result:**

Using Minitab:

Estimated Regression Coefficients for Prediction vs reference

| Term | Coef | SE Coef | T | P |
|---|---|---|---|---|
| Constant | 0.005210 | 0.001667 | 3.125 | 0.026 |
| Scan number | -0.000417 | 0.001021 | -0.408 | 0.700 |
| Int-dis | 0.003467 | 0.001021 | 3.395 | 0.019 |
| Sample thickness (mm) | 0.001436 | 0.001021 | 1.406 | 0.219 |
| Scan number*Scan number | -0.002724 | 0.001503 | -1.812 | 0.130 |
| nt-dis*Int-dis | 0.005489 | 0.001503 | 3.652 | 0.015 |
| Sample thickness (mm)* Sample thickness (mm) | -0.001633 | 0.001503 | -1.087 | 0.327 |
| Scan number*Int-dis | -0.002593 | 0.001444 | -1.796 | 0.132 |
| Scan number*Sample thickness (mm) | 0.000494 | 0.001444 | 0.342 | 0.746 |
| Int-dis*Sample thickness (mm) | 0.003646 | 0.001444 | 2.525 | 0.053 |

S = 0.00288808  PRESS = 0.000381181
R-Sq = 89.50%  R-Sq(pred) = 4.06%  R-Sq(adj) = 70.61%

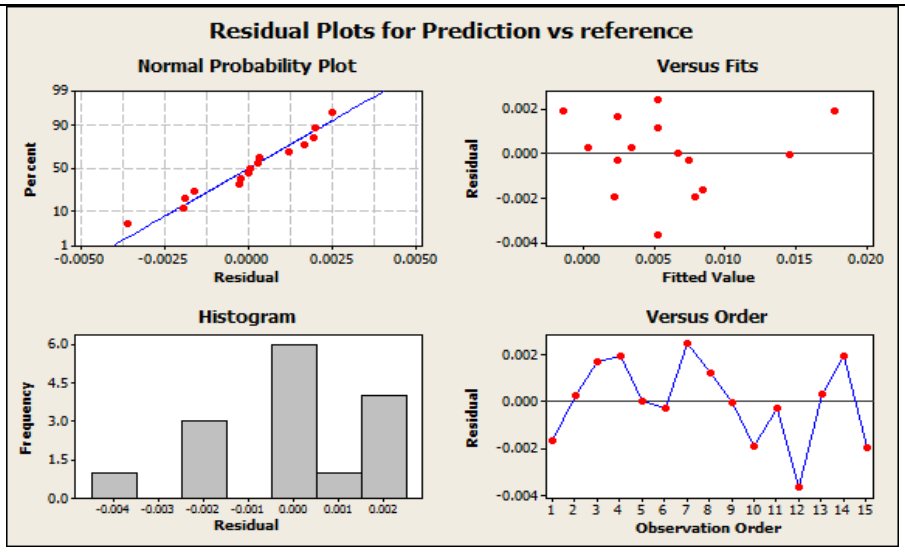


Fig 3.8. Minitab Result for Prediction vs reference difference (upper) Residual analysis for prediction reference difference (lower)

R-square adjusted of 70.61% represents a good model. Also, no pattern was found in the residual plot, this further support the fact that the model was adequate. Judging from P-value of the constant, int-dis, int-dis square is significant, interaction between int-dis and sample thickness could be significant. Therefore, the model could be simplified to:

Y(difference) = 0.00521+ 0.003467 Int-dis + 0.005489 Int-dis$^2$ + 0.003646 int-dis * sample thickness

Estimated Regression Coefficients for deviation1

| Term | Coef | SE Coef | T | P |
|---|---|---|---|---|
| Constant | 0.004234 | 0.000791 | 5.351 | 0.003 |
| Scan number | -0.000168 | 0.000485 | -0.347 | 0.742 |
| Int-dis | 0.000731 | 0.000485 | 1.509 | 0.192 |
| Sample thickness (mm) | -0.000977 | 0.000485 | -2.016 | 0.100 |
| Scan number*Scan number | -0.001928 | 0.000713 | -2.702 | 0.043 |
| Int-dis*Int-dis | 0.005490 | 0.000713 | 7.697 | 0.001 |
| Sample thickness (mm)* Sample thickness (mm) | 0.001576 | 0.000713 | 2.209 | 0.078 |
| Scan number*Int-dis | -0.001600 | 0.000685 | -2.334 | 0.067 |
| Scan number*Sample thickness (mm) | 0.000070 | 0.000685 | 0.103 | 0.922 |
| Int-dis*Sample thickness (mm) | 0.002009 | 0.000685 | 2.931 | 0.033 |

S = 0.00137074  PRESS = 0.000146678
R-Sq = 94.96%  R-Sq(pred) = 21.25%  R-Sq(adj) = 85.88%

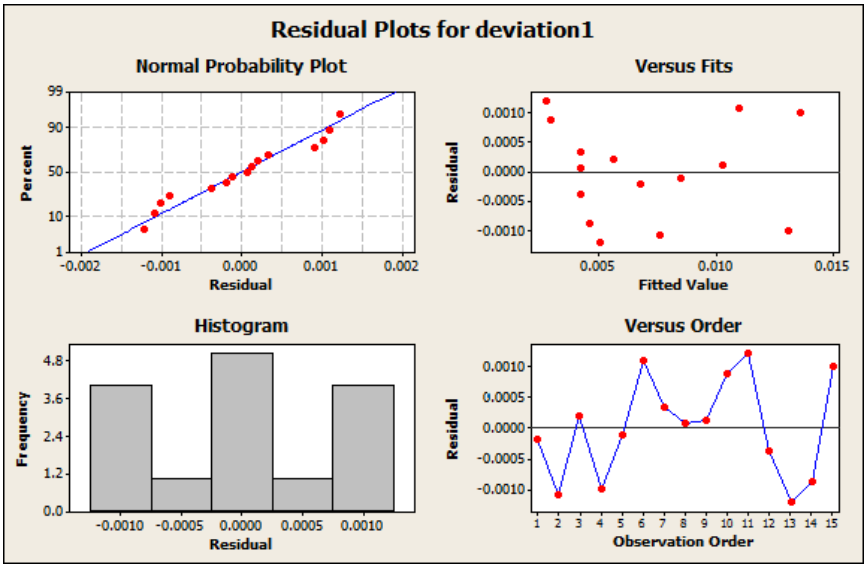


Fig 3.9. Minitab Result for Deviation (upper) Residual analysis for prediction reference difference (lower)

R-square adjusted value of 85.88% represents a good model. Judging from P-value, constant, int-dis square, int-dis thickness interaction is significant, interaction between int-dis and scan number, sample thickness square and sample thickness could be significant.As is the case with the previous model; this model can be simplified as follows:

Deviation = 0.004234 - 0.0016 Int-dis * scan number + 0.00549 Int-dis$^2$ + 0.002009 int-dis * sample thickness + 0.001576 sample thickness$^2$ – 0.000977 sample thickness

(a): (b):

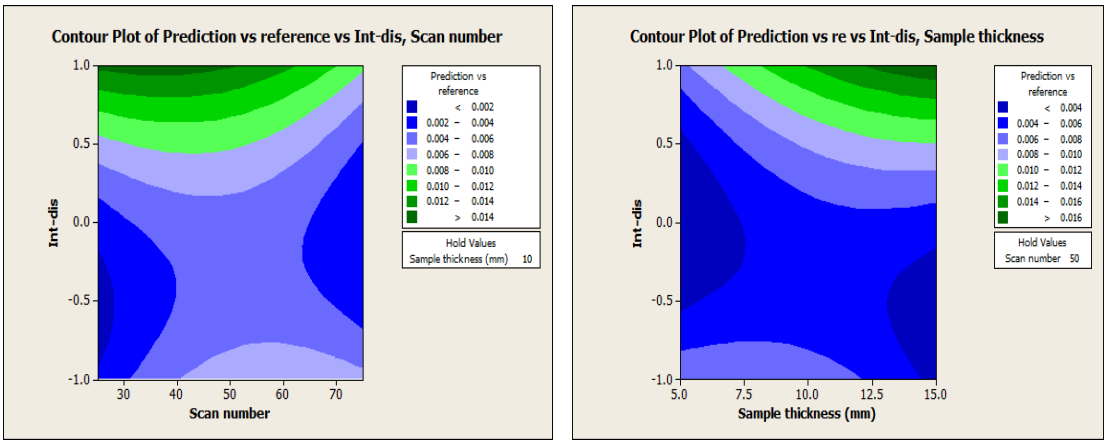


Fig 3.10. Contour plot of Y difference (a) for int-dis vs scan number (b) for int-dis vs sample thickness

Judging from figure , a saddle 3-Dimensional shape has been formed, scan number and sample thickness tend to be extreme to minimize the Y difference and int-dis is better to be lower than 0.5.

To find the operation space, overlaid plot, in which multiple responses could be discussed, is used. Time consumption (product of integration time and scan number) and deviation are also considered. First, to preserve the possibility of 24mm, 5 seconds (time consumption) is tested.

(a): (b):

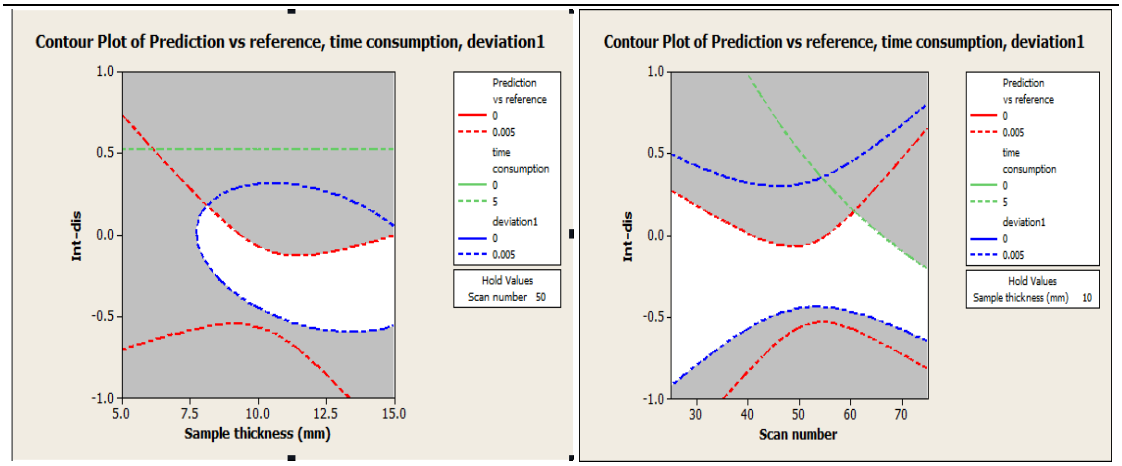


(c): (d):

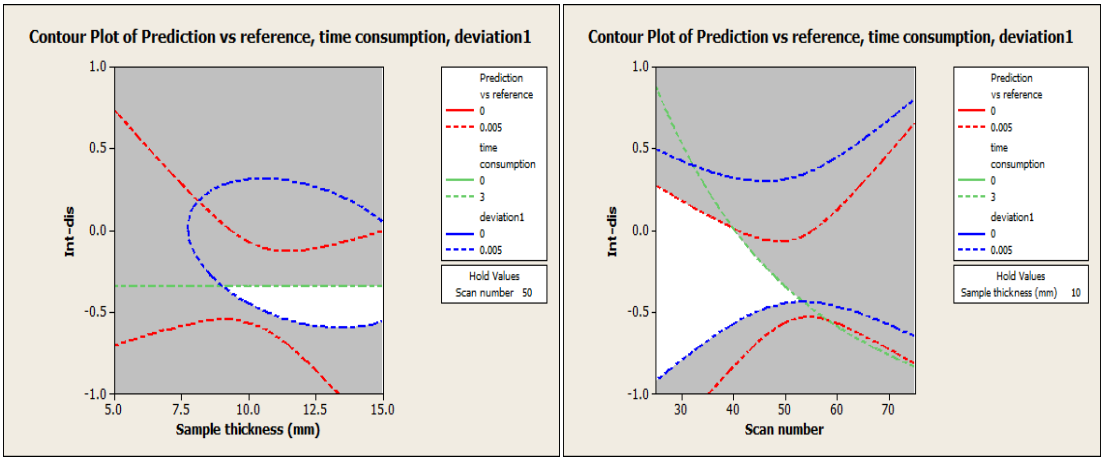


Fig 3.11. Overlaid plot for Y difference below 0.005, deviation below 0.005. (a) int-dis vs sample thickness and time consumption below 5s (b) int-dis vs scan number and time consumption below 5s (c) int-dis vs sample thickness and time consumption below 3s (c) int-dis vs scan number and time consumption below 3s

In figure 3.11, the white area is the operation space which indicates that as long as all operation variable is maintain in that area, the responses should meet the standard set up. Then by analyzing these operation area, it is found that prediction made at a distance around 12mm, with sample as thick as 15mm and having scan number of 25 will be fast and accurate. If time is not a concern, distance could range from 12 to 15mm, scan number doesn't matter at all and sample should be thicker than 7.5mm.

The conclusions coincide with the conclusion made in contour plots. Then the investigation continues with response optimizer:

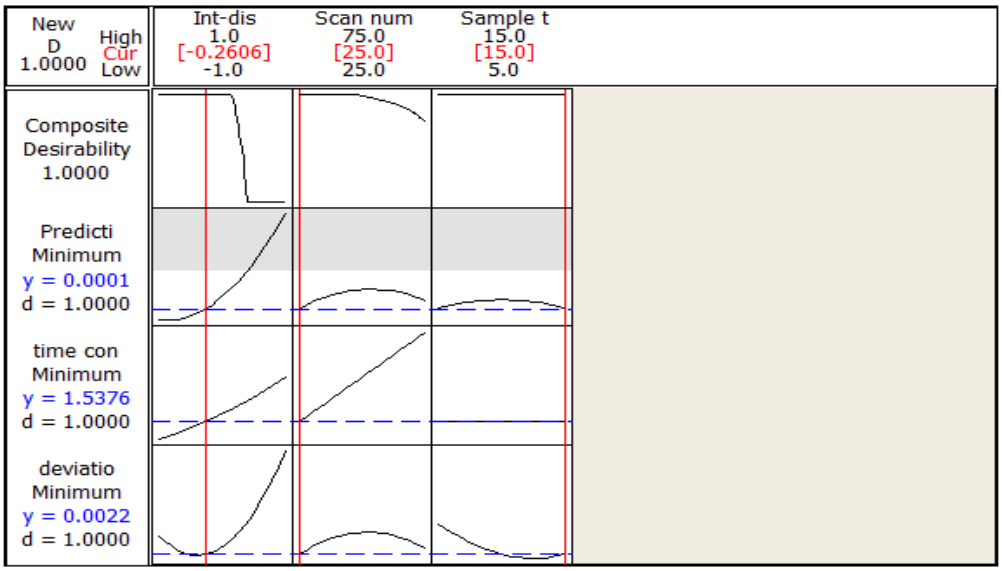


Fig 3.12. Response optimizer of all three responses

Figure 3.12 demonstrates the optimizing result by minimizing all three responses including Y difference, time consumption and deviation. The optimum operation situation suggested by it is 13.5mm distance, 15mm sample and 25 scan number, which correlate with earlier conclusions.

It is found that scan number and sample thickness are not significant while distance is significant, judging from multiple standards including P-value, response optimizer, contour plot. And the optimum operation situation suggested by this experiment is 13.5mm distance, 15mm sample and 25 scan number.

## 3.2 Effect of Place Orientation and Container Material

Certainly long distance as 15mm could prevent the dusting problem, but it may be

better if the detection could happen behind a window. If so, not only dusting problem is not in concern, a flat surface similar as static status will also be guaranteed. Therefore, the influence of window material and place orientation (side and bottom) is discussed in this part.

### 3.2.1. Pretreatment

Four kinds of pretreatment are investigated, including untreated (absorbance), SNV smoothing, Savitzky-Golay first derivative and SNV smoothing followed by Savitzky-Golay first derivative.

Table 3.9 Prediction table of Four Different treatment for 3mm detection from through plastic window (P represent prediction and D represent Deviation)

| | Untreated | | SNV | | SGolay | | SNV + SGolay | | |
|---|---|---|---|---|---|---|---|---|---|
| | P | D | P | D | P | D | P | D | Water |
| 1 | 0.3899 | 0.0018 | 0.3972 | 0.0086 | 0.3931 | 0.0046 | 0.3967 | 0.0096 | 0.3945 |
| 2 | 0.3900 | 0.0021 | 0.3981 | 0.0105 | 0.3903 | 0.0058 | 0.3973 | 0.0114 | 0.3945 |
| 3 | 0.3899 | 0.0025 | 0.3988 | 0.0127 | 0.3879 | 0.0056 | 0.3980 | 0.0138 | 0.3945 |

Judging from the values in table 3.9, it is found that the difference between prediction and reference water content is small, thus all pretreatment methods could work perfectly. Only two methods are remained to investigate in further study, which are untreated and SGolay first derivative.

### 3.2.2 Placement

Table 3.10 Prediction table of 0mm glass from bottom

| | Untreated | SGolay | Reference |
|---|---|---|---|

| Reading | Prediction | Deviation | Prediction | Deviation | Water |
|---|---|---|---|---|---|
| 1 | 0.4004501 | 0.005329238 | 0.3993078 | 0.006037337 | 0.4006 |
| 2 | 0.4012795 | 0.005687048 | 0.3994951 | 0.006442622 | 0.4006 |
| 3 | 0.4021285 | 0.005699802 | 0.3994191 | 0.006020833 | 0.4006 |

Table 3.11 Prediction table of 1.5mm glass from bottom

| | Untreated | | SGolay | | Reference |
|---|---|---|---|---|---|
| Reading | Prediction | Deviation | Prediction | Deviation | Water |
| 1 | 0.4070942 | 0.01111988 | 0.3989692 | 0.005197328 | 0.3997 |
| 2 | 0.4077427 | 0.01249038 | 0.3993989 | 0.005558177 | 0.3997 |
| 3 | 0.4092688 | 0.01093754 | 0.4005851 | 0.005221129 | 0.3997 |

Table 3.12 Prediction table of 3mm glass from bottom

| | Untreated | | SGolay | | Reference |
|---|---|---|---|---|---|
| Reading | Prediction | Deviation | Prediction | Deviation | Water |
| 1 | 0.3865935 | 0.01240089 | 0.4241832 | 0.01018791 | 0.3950 |
| 2 | 0.3901799 | 0.01514748 | 0.4262716 | 0.01026605 | 0.3950 |
| 3 | 0.3864688 | 0.01644684 | 0.4230819 | 0.01027004 | 0.3950 |

Table 3.13 Prediction table of 3mm plastic from side

| | Untreated | | SGolay | | Reference |
|---|---|---|---|---|---|
| Reading | Prediction | Deviation | Prediction | Deviation | Water |
| 1 | 0.4101674 | 0.003221418 | 0.4069191 | 0.004907767 | 0.3952 |
| 2 | 0.4089093 | 0.00265529 | 0.4077766 | 0.003268295 | 0.3952 |
| 3 | 0.4115997 | 0.002709718 | 0.4087723 | 0.003056557 | 0.3952 |

By comparing the result of table 3.10, 3.11 and 3.12, one conclusion could be made that when the prediction accuracy tend to decrease when the distance increases, and the result is best when it’s touching, however this placement is considered not application because of mechanical vibration, heating and other problem introduced by

contact. And then by comparing the result of table 3.9 and 3.13, side measurement turned out to be unreliable.

Therefore, in inline monitoring, measurement made from bottom is more desirable and should be used.

### 3.2.3 Material Comparison

Glass and plastic are discussed in this part. By comparing the result in table 3.9 to 3.12, it was found that prediction measured through plastic window, is more reliable at 3mm. However, the reason that prediction through glass window might be glass window is thicker than plastic window. Considering the higher price and difficulty of using thinner glass, the recommendation of application of plastic window at 3mm is still valid.

## 3.3 Agglomerate Size Effect

To determine whether agglomerate size will interfere the prediction result of Near Infrared prediction, Near Infrared was applied on samples with different agglomerate size.

One batch of granulation was run to obtain agglomerates with desirable size distribution. And then sieving was applied to separate agglomerates by size difference and several sets of agglomerates at same water content have been obtained as shown in figure 3.13

Fig 3.13 Agglomerate of different size

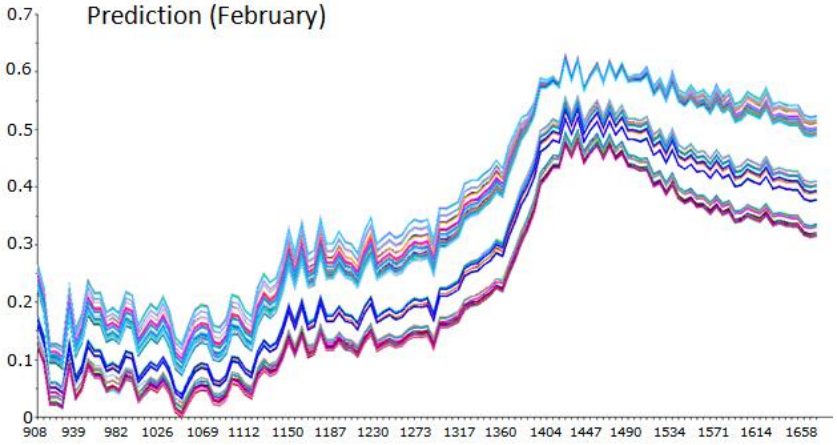


(a)

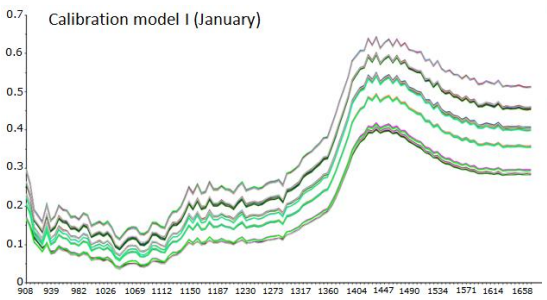


(b)

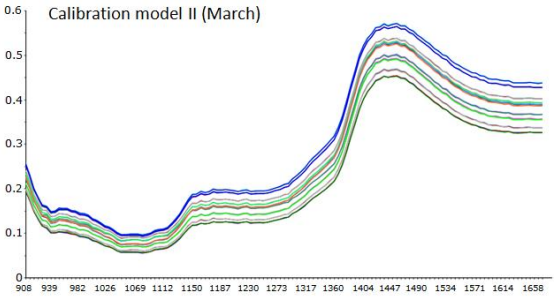


(c)

Fig 3.14 Spectra at different time. (a) Spectra for prediction taken in February (b) spectra for calibration model I taken in January (c) spectra for calibration model II taken in March

Judging from spectra in figure 3.14, different patterns have been found that spectra taken at February which is used for prediction is much more rugged (large fluctuation). All these spectra are taken at same condition including same distance, integration time and scan number, therefore the reason of these fluctuation need to be investigated. Certainly, these fluctuations significantly sabotage the prediction.

Table 3.14 Prediction table of 15mm pretreated by SNV Smoothing followed by first derivative

| Sample Size (μm) | Prediction (NIR) | Reference (LOD) | Y Difference |
|---|---|---|---|
| >2380 | 0.510457 | 0.386771 | 0.123687 |
| 1410 - 2380 | 0.528135 | 0.415347 | 0.112788 |
| 1190 - 1410 | 0.532571 | 0.419762 | 0.112809 |
| 841 - 1190 | 0.531084 | 0.416524 | 0.11456 |
| <841 | 0.515367 | 0.418495 | 0.096872 |
| powder | 0.486223 | 0.415935 | 0.070288 |

Therefore, another pretreatment method called moving average is applied to smooth the spectra as shown in figure 3.15. 3 point window is used to keep as many information as possible.

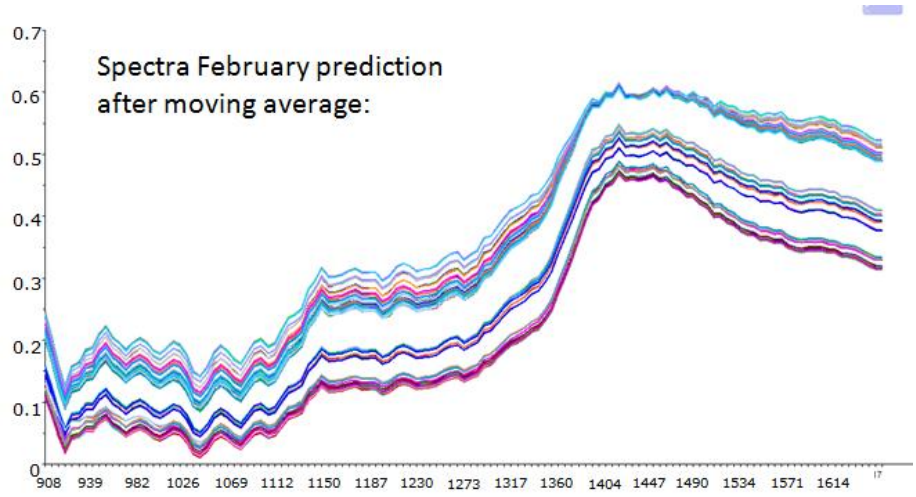

Fig 3.14 Spectra for prediction taken in February treated by three-point moving window

Table 3.14 Prediction table of 15mm pretreated by three-point moving window

| Sample Size (μm) | Prediction (NIR) | Reference (LOD) | Y Difference |
|---|---|---|---|
| >2380 | 0.334827 | 0.386771 | 0.051944 |
| 1410 - 2380 | 0.328901 | 0.415347 | 0.086445 |
| 1190 - 1410 | 0.32766 | 0.419762 | 0.092102 |
| 841 - 1190 | 0.327493 | 0.416524 | 0.089031 |
| <841 | 0.287677 | 0.418495 | 0.130818 |
| powder | 0.25602 | 0.415935 | 0.159915 |

Table 3.15 Prediction table of 15mm pretreated by three-point moving window followed by first derivative

| Sample Size (μm) | Prediction (NIR) | Reference (LOD) | Y Difference |
|---|---|---|---|
| >2380 | 0.416229 | 0.386771 | 0.029458 |
| 1410 - 2380 | 0.442791 | 0.415347 | 0.027445 |
| 1190 - 1410 | 0.451027 | 0.419762 | 0.031265 |
| 841 - 1190 | 0.44838 | 0.416524 | 0.031856 |
| <841 | 0.444017 | 0.418495 | 0.025522 |
| powder | 0.44076 | 0.415935 | 0.024825 |

Table 3.16 Prediction table of 15mm pretreated by three-point moving window and SNV followed by first derivative

| Sample Size (μm) | Prediction (NIR) | Reference (LOD) | Y Difference |
|---|---|---|---|
| >2380 | 0.38969 | 0.386771 | 0.002919 |
| 1410 - 2380 | 0.412712 | 0.415347 | 0.002635 |
| 1190 - 1410 | 0.419677 | 0.419762 | 0.000163 |

| | | | |
|---|---|---|---|
| 841 - 1190 | 0.419852 | 0.416524 | 0.003328 |
| <841 | 0.421018 | 0.418495 | 0.004278 |
| powder | 0.414067 | 0.415935 | 0.001868 |

Conclusions therefore have been made:

1. Comparing the Y difference in table 3.16, there's no significant interference introduced by agglomerate size.
2. For unknown reason, the spectra taken at different time have different pattern and the interference introduced by this could be eliminated by 3 point moving average smoothing. At this point, atmosphere temperature is suspected to be reason and further investigation is under way.
3. SNV smoothing followed by First Derivative is required to give true, accurate prediction.

## 3.4 Sample Surface Roughness effects

To determine whether surface characteristics has any effect on Near Infrared prediction, samples were made by mixing alumina with 40% of water by vortex mixer. Four samples, at different level of roughness, are prepared. Among all of them, roughness1 is the roughest one while roughness4 is the least rough one. Smooth sample is made by swiping the extra sample off of top

Table 3.17 Prediction table of 15mm roughness experiment unpretreated

| Sample ID | Prediction (NIR) | Reference (LOD) | Y Difference |
|---|---|---|---|
| rough1 | 0.233801 | 0.39125 | 0.157449 |

| | | | |
|---|---|---|---|
| rough2 | 0.241497 | 0.39148 | 0.149983 |
| rough3 | 0.248784 | 0.390373 | 0.14159 |
| rough4 | 0.238669 | 0.38977 | 0.1511 |
| smooth | 0.230995 | 0.393246 | 0.162251 |

Table 3.18 Prediction table of 15mm roughness experiment pretreated by first derivative

| Sample ID | Prediction (NIR) | Reference (LOD) | Y Difference |
|---|---|---|---|
| rough1 | 0.134577 | 0.39125 | 0.256673 |
| rough2 | 0.094796 | 0.39148 | 0.296684 |
| rough3 | 0.090543 | 0.390373 | 0.299831 |
| rough4 | 0.118859 | 0.38977 | 0.270911 |
| smooth | 0.147246 | 0.393246 | 0.246 |

Table 3.19 Prediction table of 15mm roughness experiment pretreated by SNV

| Sample ID | Prediction (NIR) | Reference (LOD) | Y Difference |
|---|---|---|---|
| rough1 | 0.396468 | 0.39125 | 0.005218 |
| rough2 | 0.395231 | 0.39148 | 0.003751 |
| rough3 | 0.392518 | 0.390373 | 0.002144 |
| rough4 | 0.395348 | 0.38977 | 0.005578 |
| smooth | 0.39625 | 0.393246 | 0.003004 |

Table 3.20 Prediction table of 15mm roughness experiment pretreated by SNV followed by first derivative

| Sample ID | Prediction | Reference | Y Difference |
|---|---|---|---|
| rough1 | 0.39784 | 0.39125 | 0.00659 |
| rough2 | 0.401952 | 0.39148 | 0.010472 |
| rough3 | 0.400483 | 0.390373 | 0.01011 |
| rough4 | 0.396661 | 0.38977 | 0.006891 |

| | | | |
|---|---|---|---|
| smooth | 0.395156 | 0.393246 | 0.00191 |

Judging from Y differences in table from 3.17 to3.20, one conclusion could be drawn that no significant difference due to surface characteristics if suitable pretreatment is applied (SNV or SNV followed by first derivative)

# Chapter 4 Offline Monitoring

## 4.1 Batch Granulation Operation

It is necessary to know the end point in granulation since it allows the design of optimal formulations, it shortens the formulation development time and minimizes problems encountered during scale-up phase product development and assures batch reproducibility and consistency. And water distribution, in another word, uniformity, could be a parameter to determine end-point.

### 4.1.1 Materials, Experiments and Method

Material: DISPERAL boehmite alumina manufactured by Sasol, purified water.

Equipment:


Figure 4.1. KG-5 high shear granulator/mixer

Method: The granulation could be divided into two stages:

The first is deagglomeration stage: In this stage, the powders are allowed to be deagglomerated at a lower set of impeller/chopper speed, which is 100/250 rpm. After two minutes, the water addition starts at a rate of 65 ml/min, and the impeller/chopper speed remains same. Usually the addition ends within seven to eight minutes, then the process steps into the second stage i.e. granulation.

Granulation stage: In this stage, the impeller/chopper speed is set at a higher rate, 500/550 rpm. The other parameters are shown in the table below:

Table 4.1. Granulation processing variables

| | | | |
|---|---|---|---|
| Solid:Liquid ratio (S:L) | 45:55 | $HNO_3$ Concentration | 0% |
| Alumina load | 300g | Flow Rate | 65ml/min |
| Mixing time | 30mins | | |
| Granulation Stage | Impeller | 300rpm | |
| | Chopper | 1500rpm | |
| Deagglomeration Stage | Impeller | 150rpm | |
| | Chopper | 500rpm | |

Table 4.1 shows the processing parameters used. The solid ratio, i.e. the ratio of alumina to water is 45:55. The peptizing agent is nitric acid, and its optimum concentration range is from 0.5% to 2%. Considering the fact that a big load is being used, 1% $HNO_3$ was decided to be a suitable concentration. However, to simplify the procedure, no peptizing agent was used for this batch. For 300g of alumina and a flow rate of 65ml/min, the mixing time was 60 minutes. Interestingly, a curious phenomenon was observed, where, the granule size increased tremendously after 50

minutes of mixing. Additionally, the NIR results (discussed in the following section) indicated that the granules had uniform water content after 36 minutes of mixing. Therefore, the optimum mixing time was reduced to ~ 45 minutes.

### 4.1.2 Results

Figure 4.2. The inside of granulator bowl during processing

Figure 4.2 shows the non-uniform premature granules after 24 minutes of mixing.

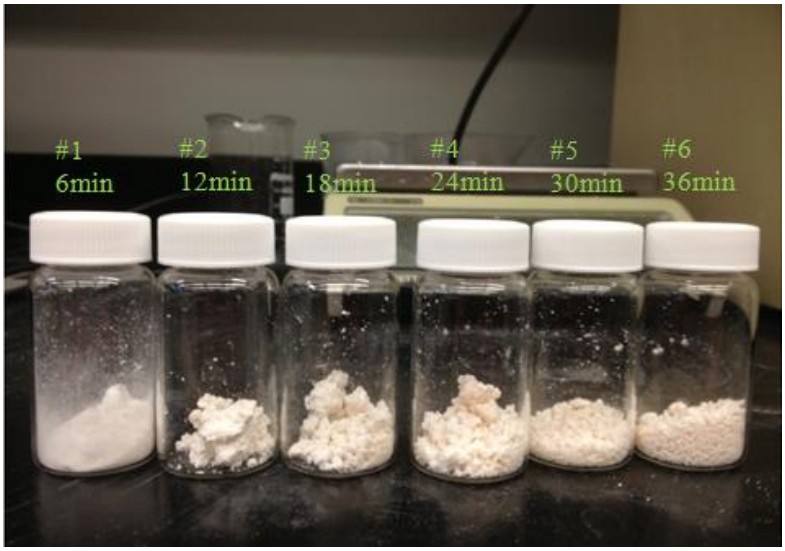


Figure 4.3. Samples shows the granulation process

Figure 4.3 shows the sample during different mixing times as they progress from fine

powder to uniform granules at 6, 12, 18, 24, 30, and 36 minutes. At first, the sample was taken immediately after water addition when it was still fine powder. Subsequently, vials 2, 3 and 4 have clear lumps, whereas in vial 5 the sample has started getting uniform and lastly, vial 6 has highly uniform granules.

## 4.2 Near Infrared Monitoring

### 4.2.1 Method

In this study, for a batch running ~ 60 mins, 30 samples were required. During the whole process, the batch was sampled ten times, with the first sampling carried out just after the water addition after which there was sampling every 6 mins until the end. Samplings were carried out at the following positions (Fig. 4.4). Samples from position 2 were used for the LOD measurements. All the samples were characterized on the Antaris NIR.

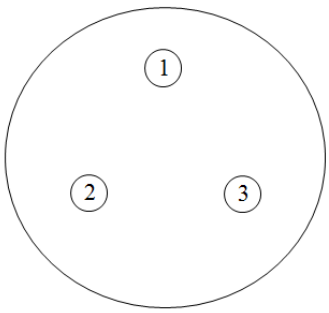


Figure 4.4. Sampling locations

### 4.2.2 Results

Table 4.2 shows the water content of different samples at the three locations

Table 4.2. Water Content of Samples

| Sample time/point | Water Content | | |
|---|---|---|---|
| | 1 | 2 | 3 |
| 6min | 0.54 | 0.57 | 0.53 |
| 12min | 0.54 | 0.54 | 0.5 |
| 18min | 0.5 | 0.53 | 0.56 |
| 24min | 0.57 | 0.55 | 0.56 |
| 30min | 0.57 | 0.54 | 0.58 |
| 36min | 0.56 | 0.55 | 0.55 |

And Figure 4.5 shows results from Table 4.2. It is clearly seen that the water content gradually becomes uniform, as was assumed. For the first three points, the difference is clear and big, after which the error shrinks and almost disappears as the end-point is approached.

The samples selected from location 2, after being measured by NIR, was subject to LOD and the results are shown in Table , These results indicate that the difference between LOD and NIR is quite small, which proves that NIR could be used to detect water content.

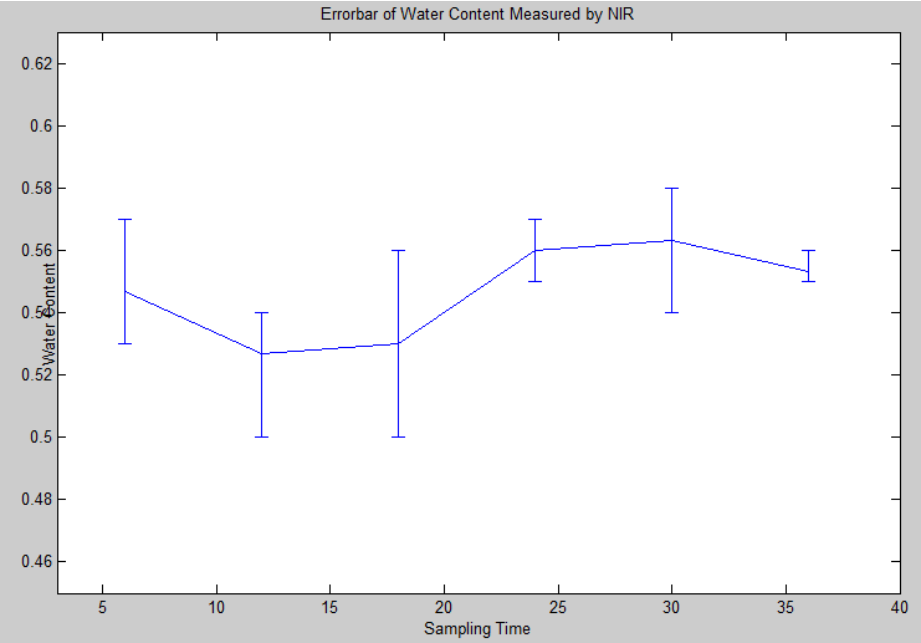


Figure 4.5. Error bar showing the water content difference between sampling points

Table 4.3. Comparison between LOD and NIR methods

| Sample time | LOD water content | NIR water content | Difference % |
|---|---|---|---|
| 18min | 0.53749 | 0.53 | 1.4126 |
| 24min | 0.54447 | 0.55 | -1.0049 |
| 36min | 0.55314 | 0.55 | 0.5709 |

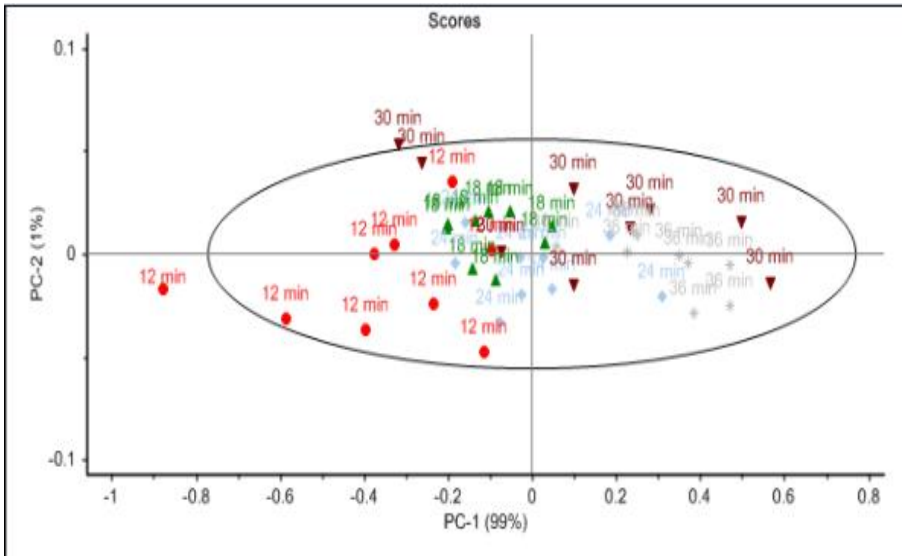


Figure 4.6. PCA result of batch mulling

All the points in Figure 4.6 are from samples collected from the three different

positions every 6 minutes. The phenomenon that points cluster together like sample collected at 36 minutes could indicates water content uniformity

# Chapter 5 Inline Monitoring setup

The inline monitoring setup is discussed as follows:

Originally, one set-up as shown in the figure 5.1 was initialed.

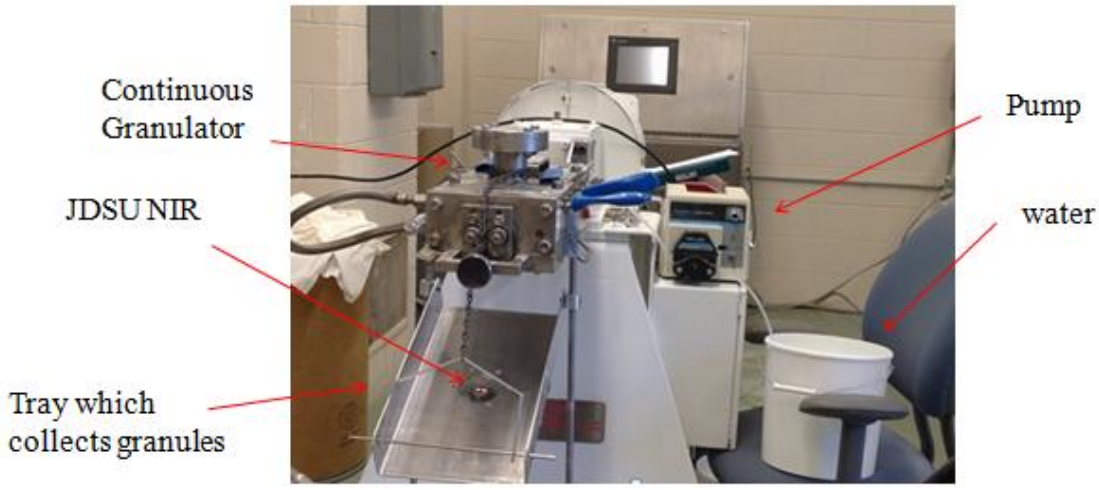


Figure 5.1 Inline monitoring set-up with tray

Water will be injected into continuous granulator, mixing with alumina powder inside to produce granules. And all these granules falls on the tray which is below the outlet of granulator and have JDSU NIR detector attached on the bottom, which is touching condition. All granules should move downward driven by gravity, and spectra are collected by IRSE (software) during this movement. And then Unscrambler Pulse (software) could interpret the spectrum freshly taken by IRSE to water content by loading a previously created model. So this system could be regarded as real time monitoring, since only several seconds are needed to get water content in sample. However, this system faces flow problems, since granules stick to the tray and even detector. And since the detector can only measure the sample which is in contact in

this system, and the sample which is in contact hardly move, thus the spectra taken by NIR couldn't represent the process at all.

Then an improved version is achieved where a conveyor is used to replace tray and detector is placed on the top, 15mm away from sample, which is shown in figure 5.2

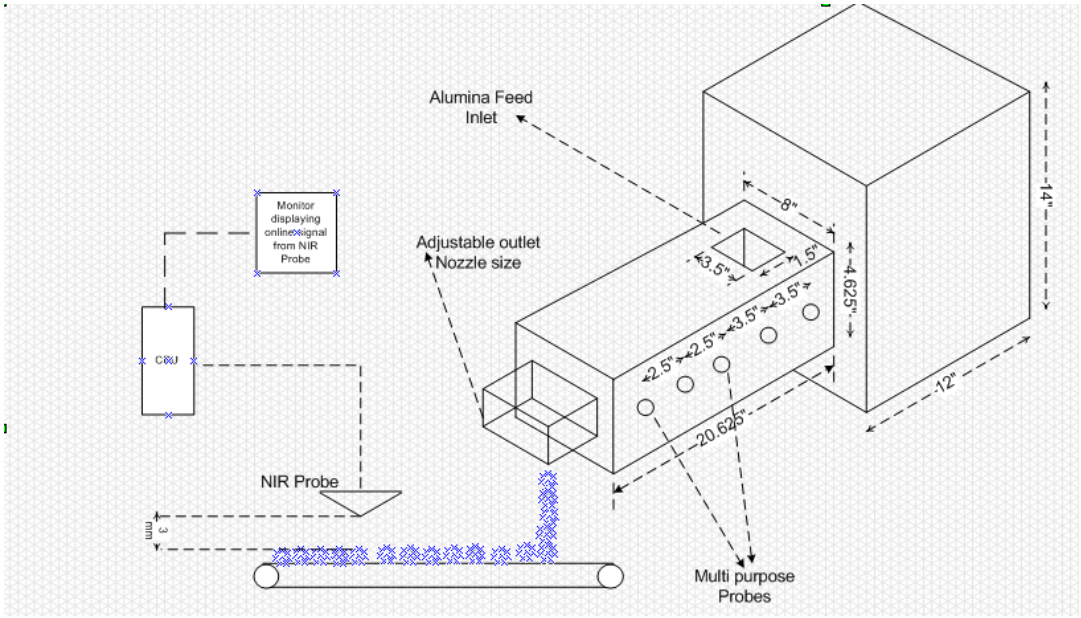


Figure 5.2 Conveyor involved inline monitoring set-up

However, another version could also be considered based on the result of 3.4. Near Infrared detector is placed 3mm below a transparent plastic conveyor while other parts are similar to the design in figure 5.2.

# Chapter 6 Conclusions and Recommendations for Future Work

In this thesis, the possibility of application of Near Infrared, a technique which could be used for substance discrimination and quantification based on perpetual molecular movement, on continuous granulation is discussed. To achieve the above goals, adequate calibration models are necessary. Many models, including those for calculating liquid content and particle size, were created. All the liquid content models passed the validation test and have close-to-1 R square and low RMSE values, which indicate adequate and reliable models. The particle size model has proven the possibility of application of NIR on particle size prediction, which could further be developed in future work. However, its high RMSE indicates the model came from a good calibration sample but the variance in sample size needs to be minimal.

Then the limit of Near Infrared operation condition from top surface was investigated. The distance between detector and sample could be increased to as far as 24 mm, thus, eliminating the dust problem. According to these results, the optimal distance is 15mm; no pretreatment method was needed to give a reliable prediction. Scan number of 25 results in a relatively fast reading (integration time for 15mm is 75000 μm, therefore one spectrum could be finished in 75000μm x 25, which is 1.875 seconds). Sample thickness has proved to be insignificant, although an optimum consistent thickness of 15mm could minimize variance.

The surface of the sample i.e. rough or smooth also has a bearing on the NIR

predictions. A rough surface does not affect prediction as long as the model is created with proper pretreatment, in this case, Savitzky-Golay first derivative with 2nd order polynomial utilizing 15 points.

Whilst investigating the effect of using a window between the sample and detector, two types of material - glass and plastic were considered instead of measuring from top is investigated. Two detection locations - side and bottom instead of top, with respect to the sample, were studied. The results from glass are not very satisfactory and as the distance between glass and the detector increases, the prediction accuracy drops significantly. Glass performs moderately at 1.5 mm but at 3mm is not reliable. However, the results from plastic look more promising, which give good results at both 1.5 mm and 3mm. This may be due to the difference in thickness of the two materials. Since it is not very feasible to obtain glass that is considerably thin, plastic could prove to be a cost effective alternative. Allowing the detector to come in direct contact with the glass/plastic surface is not advisable as a host of other problems in the form of mechanical vibrations, thermal effects could result in inaccurate NIR readings. Measurements taken from the bottom of the sample give more accurate results than those taken from the side.

NIR spectroscopy gives a way to determine process end-point by monitoring water uniformity. This could be done either by making predictions or classifying samples from different locations by principal components analysis scores plots.

Two different setups for online monitoring have been suggested. The first involves

measuring from top, while the distance is 15mm between the sample on a conveyor and detector and an overhead fence placed in front of detector could give an even surface to sample. The second setup would be measuring from the bottom, 3mm away from a conveyor that is made of a plastic material. In the latter setup the detecting surface would be flat.

The scope to further this study is tremendous. The ultimate goal could be set to continuously manufacture extrudable alumina granules that have satisfactory porosity with Near Infrared and other process analytical technology tools to control process. Obviously, water significantly affects extrudability, but other parameters could also have a serious influence. Once all the parameters affecting extrudability and porosity have been determined, suitable analytical techniques could be customized. As an example, confocal NIR microscopy could be used for off-line primary particle size detection. These techniques could then be transferred accordingly for continuous granulation to control process.

# Reference


1. Barbaro, Pierluigi, and Francesca Liguori. "Heterogenized homogeneous catalysts for fine chemicals production." *Catalysis by Metal Complexes* 33 (2010) 81-82.

2. De La Ree, Ana, and Aloysius F. Hepp. *Characterization of Catalyst Materials for Production of Aerospace Fuels*. National Aeronautics and Space Administration, Glenn Research Center, 2012.

3. LUO Sha, WU Nan, ZHOU Bo, HE Song-Bo, QIU Jie-Shan and SUN Cheng-Lin. “Effect of alumina support on the performance of Pt-Sn-K γ-alumina catalyst in the dehydrogenation of isobutene”, *Journal of Fuel Chemistry and Technology*, 41 (2013): 1481-1487

4. Li, Qiang, et al. "Alumina incorporated with mesoporous carbon as a novel support of Pt catalyst for asymmetric hydrogenation." *Catalysis Communications* 42 (2013): 68-72.

5. Paola Riani, Gabriella Garbarino, Mattia Alberto Lucchini, Fabio Canepa, Guido Busca, “Unsupported versus alumina-supported Ni nanoparticles as catalysts for steam/ethanol conversion and CO2 methanation”, *Journal of Molecular Catalysis A: Chemical,* 383-384 (2014): 10-16

6. Fonteyne, Margot, et al. "Real-time assessment of critical quality attributes of a continuous granulation process." *Pharmaceutical development and technology* 18.1 (2013): 85-97.

7. Martínez, Lizbeth, et al. "Use of near-infrared spectroscopy to quantify drug content on a continuous blending process: Influence of mass flow and rotation speed variations." *European Journal of Pharmaceutics and Biopharmaceutics* 84.3 (2013): 606-615.

8. Händle, Frank. *Extrusion in ceramics*. Springer, 2007. 161

9. Bakeev, Katherine A., ed. *Process analytical technology: spectroscopic tools and implementation strategies for the chemical and pharmaceutical industries*. John Wiley & Sons, 2010.

10. Mattes, Robert A., Denise E. Root, and Andrew P. Birkmire. "In-line Process Analysis of Residual Moisture in a Fluid Bed Granulator–Dryer Using NIR Spectroscopy." *Spectroscopy* (2005).
11. Rantanen, Jukka, et al. "Use of the near-infrared reflectance method for measurement of moisture content during granulation." *Pharmaceutical development and technology* 5.2 (2000): 209-217.
12. Sulub, Yusuf, et al. "Real-time on-line blend uniformity monitoring using near-infrared reflectance spectrometry: a noninvasive off-line calibration approach." *Journal of pharmaceutical and biomedical analysis* 49.1 (2009): 48-54.
13. Rantanen, Jukka, and Jouko Yliruusi. "Determination of Particle Size in a Fluidized Bed Granulator With a Near Infrared Set‐up." *Pharmacy and Pharmacology Communications* 4.2 (1998): 73-75.